Mon. Not. R. Astron. Soc. **398,** 255–262 (2009) doi:10.1111/j.1365-2966.2009.15092.x

An intermediate black hole spin in the NLS1 galaxy SWIFT J2127.4+5654: chaotic accretion or spin energy extraction?

G. Miniutti,[1⋆] F. Panessa[2] A. De Rosa,[2] A. C. Fabian,[3] A. Malizia,[4] M. Molina,[5] J. M. Miller[6] and S. Vaughan[7]

[1]*LAEX, Centro de Astrobiologia (CSIC–INTA); LAEFF, PO Box 78, E–28691, Villanueva de la Cañada, Madrid, Spain*
[2]*IASF/INAF, via del Fosso del Cavaliere 100, I-00133 Roma, Italy*
[3]*Institute of Astronomy, Madingley Road, Cambridge CB3 0HA*
[4]*IASF/INAF, via Gobetti 101, I-40129 Bologna, Italy*
[5]*IASF/INAF, via Bassini 15, I–20133 Milano, Italy*
[6]*Department of Astronomy, University of Michigan, 500 Church Street, Ann Arbor, MI 48109, USA*
[7]*X-ray Astronomy Group, University of Leicester, LE1 7RH Leicester*

Accepted 2009 May 18. Received 2009 May 18; in original form 2009 March 12

ABSTRACT

We have observed the hard X-ray selected Narrow-Line Seyfert 1 galaxy SWIFT J2127.4+5654 with *Suzaku*. We report the detection of a broad relativistic iron emission line from the inner accretion disc. Partial covering by either neutral or partially ionized gas cannot reproduce the spectral shape and, even if its presence is assumed, it does not significantly change the inferred broad-line parameters. By assuming that the inner edge of the accretion disc corresponds to the innermost stable circular orbit of the black hole space–time, the line profile enables us to measure a black hole spin $a = 0.6 \pm 0.2$. However, a non-rotating Schwarzschild space–time is excluded at just above the 3σ level, while a maximally spinning Kerr black hole is excluded at the $\sim 5\sigma$ level. The intermediate spin we measure may indicate a recent merger, or that accretion-driven black hole growth in this source proceeds through short-lived episodes with chaotic angular momentum alignment between the disc and the hole rather than via prolonged accretion. The measured steep emissivity index ($q \simeq 5$) constrains the irradiating X-ray source to be very centrally concentrated. Light bending may help focus the primary emission towards the innermost accretion disc, thus steepening the irradiation profile. On the other hand, steep profiles can also be reached if magnetic extraction of the hole rotational energy is at work. If this is the case, the interplay between accretion (spinning up the black hole) and rotational energy extraction (spinning it down) forces the hole to reach an equilibrium spin value which, under standard assumptions, is remarkably consistent with our measurement. Rotational energy extraction would then be able to simultaneously account for the intermediate spin and steep emissivity profile we infer from our spectral analysis without the need to invoke chaotic accretion episodes. We also report tentative evidence for short time-scale line profile variability. The relatively low statistical significance of the variability (about 98 per cent confidence level) prevents us from drawing any firm conclusions which must be deferred to future observations.

Key words: galaxies: active – X-rays: galaxies.

1 INTRODUCTION

X-ray irradiation of dense and relatively cold material in the vicinity of accreting black holes can produce an X-ray reflection spectrum characterized by fluorescent emission lines (most notably in the iron K regime around 6–7 keV), a Compton hump around ∼20–30 keV and a soft excess below 1–2 keV. If the reflection spectrum is emitted from the inner accretion disc, the whole spectrum is distorted by relativistic effects. Relativistic emission line profiles bear the imprint of the strong Doppler and gravitational energy shifts (plus aberration and light bending) which are intrinsic to the inner disc, where velocities and gravity are the largest. Given that the iron (Fe) K emission line is strongest in the X-ray regime, relativistic Fe line studies can serve to probe the relativistic space–time close to black holes (Fabian et al. 1989, 2000; Reynolds & Nowak 2003; Fabian & Miniutti 2009).

The astrophysical black hole space–time only depends on black hole mass and spin. While the black hole mass sets the scale of the system, the spin qualitatively changes the nature of the space–time

⋆E-mail: gminiutti@laeff.inta.es

and can thus be regarded as the most crucial parameter. X-ray observations of accreting Galactic black holes and of active galactic nuclei (AGN) are now starting to attack the difficult process of measuring black hole spin through relativistic Fe line diagnostics (e.g. Brenneman & Reynolds 2006; Miller 2007; Miller et al. 2009). Measuring such an important parameter in large and statistically meaningful samples of accreting sources in the future is crucial to provide answers to several open questions in the field. For instance, such studies will allow observers to test whether a non-zero black hole spin is a necessary condition to launch relativistic jets (see e.g. Sikora, Stawarz & Lasota 2007). In Galactic sources, since accretion from the companion star is unlikely to significantly modify the spin imprinted at birth (Volonteri et al. 2005), a measure of the black hole rotation will provide crucial clues on the dynamics and black hole formation during the supernova explosion. On the other hand, the spins of supermassive black holes in AGN bear the imprints of the hole growth and evolution, and of the relative importance of (i) mergers and accretion and (ii) prolonged versus chaotic/episodic accretion in setting up the final black hole mass (e.g. Volonteri et al. 2005; Berti & Volonteri 2008; King, Pringle & Hofmann 2008).

Here we report results from a *Suzaku* observation of the bright Narrow-Line Seyfert 1 (NLS1) galaxy SWIFT J2127.4+5654, previously detected in hard X-rays by *Swift*/BAT and *INTEGRAL*/IBIS and in the soft X-ray band by the *Swift*/XRT.

2 SWIFT J2127.4+5654

SWIFT J2127.4+5654 (aka IGR J21277+5656) is a low Galactic latitude (∼4.4 degrees) hard X-ray source detected with *Swift*/BAT (Tueller et al. 2005) and later identified as an NLS1 galaxy at redshift 0.0147 based on the observed Hα full width at half-maximum (FWHM) of ∼1180 km s^{-1} (Halpern 2006). Subsequent work by Malizia et al. (2008) supported the NLS1 classification by obtaining, despite a slightly larger Hα FWHM of ∼2000 km s^{-1}, a relatively low [O III]/H$_\beta$ ratio of 0.72 ± 0.05 and significantly enhanced Fe II emission (Fe II/H$_\beta = 1.3 \pm 0.2$). Some radio-loud AGN exhibit optical spectra which display narrow permitted lines and weak [O III] emission and are so potentially misclassified as NLS1 galaxies. SWIFT J2127.4+5654 has a 20 cm flux of 6.4 mJy (Condon et al. 1998). The source appears compact, with no visible elongation in the 1.4 GHz NRAO VLA Sky Survey (NVSS), and is certainly not bright enough to be classified as a radio-loud source, so that the NLS1 classification of SWIFT J2127.4+5654 appears robust (we note anyway that the NLS1 nature of AGN and radio loudness are not necessarily mutually exclusive; see Komossa et al. 2006).

The source was detected in the hard band with *INTEGRAL*/IBIS and, although no spectral information can be extracted from a single IBIS pointing, an averaged spectrum was obtained by Malizia et al. (2008) in the 17–100 keV band by summing all the available on-source exposures, resulting in a steep spectrum (Γ in the range 2.4–3) and a hard X-ray flux of 2.46×10^{-11} erg s^{-1} cm^{-2} in the 20–100 keV band. The *Swift*/XRT data (two observations for a total of ∼10 ks) have been analysed by Malizia et al. (2008) in conjunction with the *INTEGRAL*/IBIS averaged spectrum. The main result of this analysis is that the softer X-rays probed by *Swift*/XRT exhibit a much flatter and more typical spectral slope of $\Gamma \sim 1.9$ suggesting a more complex broad-band spectral shape than a simple power law. Although the averaged *INTEGRAL*/IBIS high-energy data may be affected by variability, the analysis suggests the presence of a spectral break or of an exponential cut-off in the range of 20–50 keV. If the continuum is assumed to originate from inverse Compton of the soft disc photons in a hot corona, a low-energy cut-off in that energy range implies a low temperature of the Comptonizing plasma (about 10–20 keV). On the other hand, other interpretations are viable: for instance, the broad-band X-ray spectrum may be characterized by the presence of a relatively steep continuum plus a harder reflection component and/or absorption leading to the observed apparent spectral break in the hard X-ray band.

3 THE *SUZAKU* OBSERVATIONS

Suzaku observed SWIFT J2127.4+5654 on 2007 December 9 for a total net exposure of 92 ks. SWIFT J2127.4+5654 was placed at the HXD nominal position. Here we consider data from the XIS (Koyama et al. 2007) and HXD/PIN (Takahashi et al. 2007) detectors. During our observation, the front-illuminated CCD XIS 0 was not operating properly and, after the loss of XIS 2, the only available CCD spectra are those provided by the back-illuminated XIS 1 and the front-illuminated XIS 3. We analyse the v2.2 data and we use the HEASOFT 6.5 distribution and associated CALDB released on 2008-08-11. All spectra we use are grouped to a minimum of 50 counts per bin. We use the χ^2 minimization technique and we quote 90 per cent errors on model parameters unless specified otherwise. Spectral analysis is performed with the XSPEC v 12.5 software (Arnaud 1996; Dorman & Arnaud 2001). Luminosities are computed by assuming a Λ cold dark matter cosmology with $H_0 = 70\,\mathrm{km\,s^{-1}}$, $\Omega_\Lambda = 0.73$ and $\Omega_\mathrm{M} = 0.27$.

4 THE *SUZAKU* VIEW OF SWIFT J2127.4+5654

We first consider the XIS 1 and XIS 3 time-averaged spectra in the 0.5–10 keV (XIS 3) and 0.5–8 keV (XIS 1) band, ignoring the 1.75–1.95 keV energy range because of remaining uncertainties in the instrumental Si edge region and because we see in the data a suspect sharp spectral feature not accounted for by the current calibration. The spectra are fitted jointly with a simple absorbed power-law model. We use a $z = 0$ photoelectric absorption model (PHABS) with column density fixed at the Galactic value (∼7.7×10^{21} cm^{-2}; Kalberla et al. 2005) and a further intrinsic column N_H^z at the redshift of the source (using the ZPHABS model). Abundances are set to Wilms, Allen & McCray (2000) and we use photoelectric absorption cross-sections from Balucinska-Church & McCammon (1992). The model provides a reasonable description of the data [2881 for 2670 degrees of freedom (d.o.f.)] and we measure $N_\mathrm{H}^z = 2.9 \pm 0.1 \times 10^{21}$ cm^{-2} with photon index $\Gamma = 1.98 \pm 0.02$. Replacing the intrinsic neutral absorber with an XSTAR-based ionized one[1] does not improve the fit and the ionization parameter is constrained to be $\log \xi \leq -0.5$.

Our spectral best-fitting model is a fair statistical description of the data, but leaves however clear residuals as shown in Fig. 1. The most important residuals are in the Fe K band around 6 keV and suggest the presence of a broad Fe line. On the other hand, some spectral curvature is also suggested by the soft X-ray data below about 2 keV possibly indicating a small soft excess (where 'small' should however take into account the high observed column density which would mask anyway a larger soft excess). Below 1 keV, we

[1] We use the XSTAR code included in the HEASOFT 6.5 distribution to build an ionized absorber XSPEC table model (Bautista & Kallman 2001). We assume a $\Gamma = 2$ continuum between 0.1 and 1000 Ry, and a turbulent velocity of 200 km s^{-1}. The column density ranges between 0.5 and 50×10^{21} cm^{-2}, while $\log \xi$ ranges between −1 and 2.5.

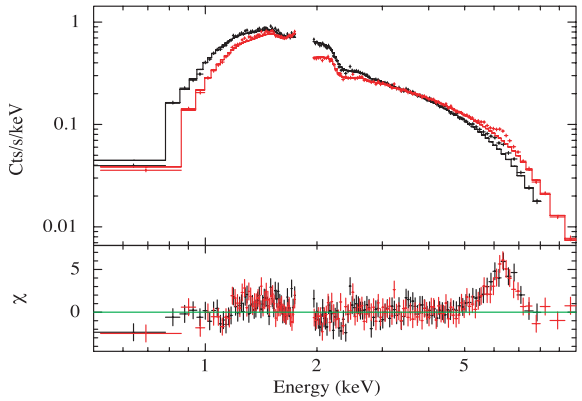

Figure 1. XIS 1 and XIS 3 spectra, model and residuals for a simple absorbed power-law fit. The data are re-binned for visual clarity only.

also note the possible presence of excess absorption which is not accounted for by the current spectral model.

We first consider the possible presence of a soft excess by introducing a multicolour blackbody model (DISKBB; see Makishima et al. 1986). The quality of the fit improves significantly ($\chi^2 = 2755$ for 2668 d.o.f., i.e. $\Delta\chi^2 = -126$ for Δd.o.f. $= -2$) and we obtain an inner disc temperature of 340 ± 40 eV with photon index $\Gamma = 1.92 \pm 0.03$ and $N_{\rm H}^{z} = 3.8 \pm 0.2 \times 10^{21}\,{\rm cm}^{-2}$. We point out that such a high blackbody temperature is unphysical and cannot be associated with thermal emission from the accretion disc (which peaks in the UV) so that the blackbody model has to be considered as phenomenological. Given the different soft spectral shape, we re-investigate the presence of an ionized intrinsic absorber. Using the same XSTAR model as discussed above, we replace the intrinsic neutral absorber with an ionized one, and we obtain a statistical improvement ($\chi^2 = 2732$ for 2667 d.o.f.) with low ionization parameter $\log\xi = 0.15 \pm 0.10$ and $N_{\rm H}^{z} = 6.6 \pm 0.5 \times 10^{21}\,{\rm cm}^{-2}$. The disc blackbody component has now a temperature of $\sim$240 eV (still too hot to represent the high-energy tail of the disc thermal emission) and it contributes by about 20 per cent to the total unabsorbed luminosity in the 0.5–2 keV band, in line with the typical $\sim$30 per cent soft excess contribution in Seyfert 1 galaxies and type I quasars, e.g. Miniutti et al. (2009).

The above modelling provides a good description of the soft X-ray data, but the main positive residuals in Fig. 1 in the Fe *K* band are not accounted for yet. To model the residuals around 6 keV, we introduce a Gaussian emission line with energy, width and normalization free to vary. The Gaussian emission line provides a further very significant improvement of the statistical quality of the fit, with a $\Delta\chi^2 = -165$ for Δd.o.f. $= -3$($\chi^2 = 2567$ for 2664 d.o.f.). The Gaussian line has an energy of 6.35 ± 0.10 keV, consistent with neutral Fe Kα emission, and is resolved with a relatively large width of $\sigma = 0.53 \pm 0.10$ keV.

Given that a narrow Fe Kα line (most likely originating from distant reflection) is almost ubiquitous in the X-ray spectra of AGN (e.g. Bianchi et al. 2009), we also add a narrow Gaussian emission line with energy $E \equiv 6.4$ keV and width $\sigma \equiv 1$ eV. The narrow Fe line does not improve very significantly the quality of the fit ($\Delta\chi^2 = -4$ for 1 d.o.f. less than before) but we keep it for consistency, measuring a line intensity of $4.6^{+4.0}_{-4.1} \times 10^{-6}\,{\rm ph\,s^{-1}\,cm^{-2}}$. The broad line has an equivalent width (EW) of 220 ± 50 eV, while the narrow Fe line EW is 15 ± 10 eV. Adding narrow Fe XV and/or Fe XVI emission/absorption lines in the Fe *K* band does not improve the fit significantly and does not change the broad Fe Kα line parameters at all. The best-fitting parameters for our final model are given in Table 1.

Table 1. Best-fitting parameters for the joint fit of XIS 1 and XIS 3 data. N_H^z and $\log\xi^z$ refer to the intrinsic ionized absorber at the redshift of the source, while the subscripts BL and NL refer to the broad and narrow Gaussian emission lines in the Fe *K* band.

Γ	2.06 ± 0.03
$N_H^{z,a}$ [cm^{-2}]	6.6 ± 0.5
$\log\xi^{z,a}$	0.15 ± 0.10
$kT_{\rm inn}$ [eV]	240 ± 20
$E_{\rm BL}$ [keV]	6.35 ± 0.10
$\sigma_{\rm BL}$ [keV]	0.53 ± 0.10
$EW_{\rm BL}$ [eV]	220 ± 50
$EW_{\rm NL}$ [eV]	15 ± 10
F_X^b [erg s^{-1} cm^{-2}]	3.29 ± 0.03
L_X^c [erg s^{-1}]	1.74 ± 0.01
$L^d_{\rm Bol}/L_{\rm Edd}$	$\simeq$0.18
χ^2/d.o.f.	2563/2663

[a] N_H^z denotes the column density of the intrinsic absorber at $z = 0.0147$ in units of $10^{21}\,{\rm cm}^{-2}$, while its ionization parameter (ξ^z) is in units of erg cm s^{-1}; [b] absorbed X-ray flux in the 2–10 keV band in units of $10^{-11}\,{\rm erg\,s^{-1}\,cm^{-2}}$; [c] unabsorbed X-ray luminosity in the 2–10 keV band in units of $10^{43}\,{\rm erg\,s^{-1}}$; [d] We compute $L_{\rm Bol}$ from the 2–10 keV X-ray luminosity applying the Marconi et al. (2004) bolometric correction. We assume a black hole mass of $1.5 \times 10^7\,{\rm M}_\odot$ (Malizia et al. 2008).

Broad Fe lines are sometimes claimed to be a spurious effect due to complex absorption (e.g. Turner & Miller 2009). In particular, partial covering scenarios potentially introduce hard X-ray spectral curvature which can be misinterpreted as a broad Fe line. As a sanity check, we then add a partial covering ionized absorber to our model (the ZXIPCF model in XSPEC). However, the partial covering absorber does not improve the statistical quality of the fit ($\chi^2 = 2561$ for 2660 d.o.f.) and no constraints other than a small covering fraction of less than 20 per cent can be obtained. We obtain the same unconstrained result if a neutral partial coverer is used instead. Moreover, no significant variation in the broad-line parameters is seen in either case (new parameters are $E = 6.36 \pm 0.11$ keV, $\sigma = 0.51 \pm 0.12$ eV for a line EW$\simeq$ 210 eV for both attempts). Replacing the broad Fe line with the ionized or neutral partial covering model and re-fitting the data produce a much worse description of the data (the minimum $\Delta\chi^2$ being $\Delta\chi^2 = +56$ with the neutral partial coverer with respect to the best fit with broad line and no partial covering). We then conclude that the detection of a broad Fe line in the X-ray spectrum of SWIFT J2127.4+5654 is robust against partial covering scenarios irrespectively of the absorber ionization state.

4.1 The relativistic Fe line: a probe of black hole spin

Having established that a broad Fe line is present in the data with high statistical significance, we now investigate its nature in some more detail. The most likely origin for the broad Fe line is reflection off the inner accretion disc. Relativistic line models depend on several parameters, namely the inner and outer disc radii, the disc-observer inclination, and the shape of the emissivity profile (plus line energy and normalization). The emissivity is generally assumed

to be axisymmetric and with a power law ($\epsilon \propto r^{-q}$, where q is the emissivity index) or broken power-law shape.

The inner disc radius is of particular interest. Under the hypothesis that the reflecting disc is truncated at the innermost stable circular orbit (ISCO) around the black hole (see Reynolds & Fabian 2008 for a recent discussion), the inner disc radius only depends on the black hole spin. Relativistic line models in which the black hole spin is a variable free parameter are now available (the KYRLINE and KERRDISK models; Dovčiak, Karas & Yaqoob 2004a; Brenneman & Reynolds 2006, respectively). These models work under the assumption that the inner disc radius is identified with the ISCO and compute the orbital motion self-consistency (as opposed to the cases of the DISKLINE and LAOR models which assume a particular black hole spin, see Fabian et al. 1989; Laor 1991). After checking that results from the KYRLINE and KERRDISK models are consistent with each other in terms of statistics, best-fitting values, and errors on the parameters, we report results for the KYRLINE model only.

We replace the broad Gaussian Fe line of our previous model with the KYRLINE relativistic line. We assume a neutral Fe line at 6.4 keV, as suggested by previous results (see Table 1), and we fix the outer disc radius to 400 r_g, while black hole spin, emissivity index q and disc inclination i are free to vary. We keep the ionized absorber, disc blackbody, power law and narrow Fe K line components as before (all parameters free to vary except for the narrow Fe line energy and width fixed at 6.4 keV and 1 eV respectively). The Fe line model is better physically motivated than the broad Gaussian used above, and provides a similar (although not a better) statistical quality with χ^2/d.o.f. $= 2561/2662$, to be compared with χ^2/d.o.f. $= 2563/2663$ when the broad Gaussian model was used. We measure $q = 5.2^{+1.8}_{-1.2}$, $i = 46^\circ \pm 4^\circ$, and a black hole spin of $a = 0.66^{+0.12}_{-0.09}$.

In Fig. 2, we show $\Delta\chi^2$ contours for the emissivity index q and the black hole spin, demonstrating that the parameter space is constrained. If we consider $\sim 3\sigma$ errors for the two parameters (i.e. $\Delta\chi^2 = 11.83$), the black hole spin is constrained to be $a = 0.66 \pm 0.16$. Finally, we have re-fitted the data by forcing the spin to be either $a = 0$ or $a = 0.998$, corresponding to a Schwarzschild and a maximally spinning Kerr space–time, respectively. We obtain $\Delta\chi^2 = +13$ for $a = 0$ and $\Delta\chi^2 = +15$ for $a = 0.998$, meaning that both extremes are rejected at the $\sim 3\sigma$ level only.

The emissivity index we measure is steep and suggests that Fe emission is concentrated in the very inner regions of the disc. If the

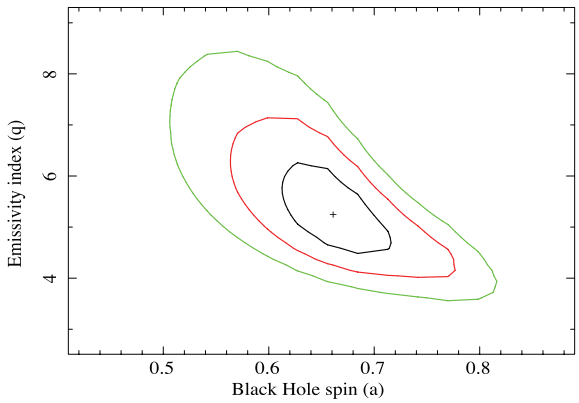

Figure 2. $\Delta\chi^2 = 2.30$, 6.17 and 11.83 contours (corresponding to approximate 68.3, 95.4 and 99.7 per cent confidence regions) for the two most relevant relativistic blurring parameters, namely black hole spin (a) and emissivity index (q).

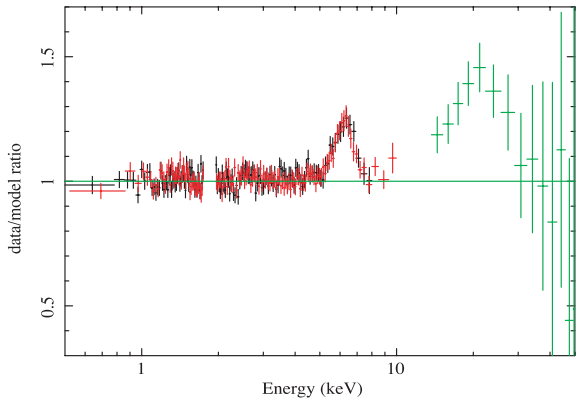

Figure 3. The best-fitting continuum model is applied to the broad-band data. The Fe K band region has been ignored in the fit. Besides the broad Fe line, the ratio also highlights positive residuals around 20 keV which indicate the likely presence of a Compton hump associated with the reflection continuum.

irradiating X-ray source is point-like, ray-tracing studies in the Kerr geometry reveal that the irradiating profile cannot be that steep out to the largest radii (e.g. Miniutti & Fabian 2004). A more physically plausible irradiating profile can be approximated with a broken power law with a steep index out to a break radius, and reaching its asymptotic al r^{-3} behaviour at larger radii. Such emissivity profile was indeed used by several authors to model the highest signal-to-noise ratio relativistic Fe line known so far in AGN, that of MCG–6-30-15 (Fabian et al. 2002; Brenneman & Reynolds 2006; Miniutti et al. 2007). We then try to fit the data by using the KERRDISK model which allows the user to define a broken power-law emissivity. We could not find any statistical improvement by using such model, and the outer emissivity index is always consistent with the inner one. A solution with $q_{\rm in} \sim 5$ out to a break radius of 5–10 r_g and $q_{\rm out} \equiv 3$ at larger radii is however statistically equivalent to the one presented above and possibly more physically motivated. Since this solution cannot be explored in detail due to signal-to-noise ratio limitations, we prefer to continue our analysis with the simpler non-broken power-law emissivity profile discussed above.

The relativistic line model best-fitting parameters we infer should be taken with care. In fact, the broad Fe line must be associated with a whole X-ray reflection continuum which, by changing the underlying spectral shape, may affect the derived parameters (certainly reducing the line EW). Since the reflection continuum is characterized by a Compton hump showing up in the hard X-rays around 20 keV, we proceed to include the HXD data in the attempt to build a more self-consistent model.

4.2 Including the high-energy *HXD/PIN* data

Suzaku's HXD and, in particular, the PIN detector is well suited to investigate the presence of a reflection component in the spectrum because of the good sensitivity up to 40–50 keV. We thus consider the 14–50 keV PIN data, and we introduce a cross-normalization factor of 1.17 ± 0.02 between the PIN and the XIS 3, rescaling the recommended value[2] of 1.181 ± 0.016 which is valid for the XIS 0 (not available here) at the HXD nominal position taking into account the XIS 3 to XIS 0 cross-normalization constant of 1.009 ± 0.011. In Fig. 3, we show the data to model ratio when the previous

[2] See Ishida et al., 2008-06-26, JX–ISAS–SUZAKU–MEMO–2008-06.

continuum model is applied to the broad-band data. The residuals clearly show, besides the broad Fe line, positive residuals in the PIN band, most likely associated with the expected Compton hump.

To test the Compton hump nature of the hard X-ray residuals, we replace the power-law continuum of our previous model with a power law plus reflection continuum model, assuming reflection off a neutral slab of gas (the PEXRAV model). We force the metal abundances to be solar, and we fix the inclination of the reflector to 46°, as suggested by the relativistic line fits discussed above. Although the reflection model is not self-consistent because it does not include line emission, it is useful to constrain the strength of the reflection continuum and to search for a high-energy cut-off below ∼50 keV as suggested by Malizia et al. (2008) in their analysis of the combined *Swift* and *INTEGRAL* data.

We obtain a very good description of the broad-band data ($\chi^2 = 2680$ for 2755 d.o.f.) and the hard residuals shown in Fig. 3 disappear. The photon index is in line with our previous result ($\Gamma = 2.10 \pm 0.06$) and the relative contribution of the reflection component (i.e. the reflection fraction R) is measured to be $R = 1.0^{+0.5}_{-0.4}$. As for the high-energy cut-off at energy E_c, we obtain $E_c \geq 35$ keV, only marginally consistent with the result by Malizia et al. (2008). As expected, the inclusion of the reflection continuum reduces the broad Fe line EW (now ∼150 eV), while the narrow Fe line EW is ∼16 eV making the total EW associated with the Fe lines broadly consistent with the theoretical expectations for solar Fe abundance in the case of neutral matter (e.g. George & Fabian 1991). As for the other broad-line parameters, our results are consistent with those reported above. In particular, the disc emissivity is $q = 5.2^{+1.6}_{-1.3}$ and the black hole spin is $a = 0.64 \pm 0.18$, confirming our previous estimate and demonstrating that the reflection component does not affect the relativistic blurring parameters significantly in this case.

4.3 A self-consistent disc reflection model

In order to attempt to model the data, and in particular the reflection component, as self-consistently as possible, we use the ionized reflection model from Ross & Fabian (2005) where fluorescent emission lines and reflection continuum are computed together. Moreover, given the evidence for a broad Fe line, we convolve the whole rest-frame reflection spectrum with the relativistic kernel KYCONV, which extends the relativistic blurring of the KYRLINE model to any intrinsic spectrum. The reflection model we use is computed by assuming a power-law continuum with fixed high-energy cut-off at 100 keV, but it is a pure reflection model and does not include the illuminating continuum. We then model it by using a cut-off power-law continuum with $E_c \equiv 100$ keV for consistency.

Ionized reflection naturally produces also a soft X-ray excess with respect to the underlying power-law continuum for a wide range of ionization states. Hence, we start our analysis by removing the blackbody component from our spectral model in the attempt of fitting the whole broad-band data with the most self-consistent model, comprising just an absorbed power law (Galactic plus intrinsic ionized absorption as before) plus disc reflection (keeping however the narrow Fe Kα line as before). The model has then 3 d.o.f. more than the previous one. The ionization state of the reflector, which sets the general spectral shape and the Fe line energy, is free to vary in the fit, while we first fix the Fe abundance to the solar value.

The model provides a good representation of the data ($\chi^2 = 2728$ for 2758 d.o.f.) but the previous model was statistically slightly better. The most notable difference is that the ionized absorber tends to the lowest ionization state allowed by our table model ($\log \xi = -1$). We then replace it with a neutral intrinsic absorber using the ZPHABS model and we obtain a significant improvement ($\chi^2 = 2707$ for 2759 d.o.f.) measuring $N_{\rm H}^{\rm z} \simeq 4.5 \times 10^{21}$ cm^{-2}. Given that the soft excess is now described with disc reflection as opposed to the phenomenological blackbody model discussed above, changes in the absorber properties are not very surprising. However, the issue of whether the intrinsic absorber is neutral or slightly ionized is not completely settled in our opinion, and future high-resolution data are required to resolve individual absorption features. Letting the Fe abundance free to vary produces a further improvement with a final result of ($\chi^2 = 2690$ for 2758 d.o.f.) with $A_{\rm Fe} \simeq 1.5$ times the solar value (see Table 2 for a summary of the best-fitting parameters).

Table 2. Best-fitting parameters for the power law plus relativistically blurred reflection model (also comprising an additional narrow Fe Kα line).

Γ	2.12 ± 0.09
$N_H^{z,a}$ [cm^{-2}]	4.5 ± 0.9
i [degrees]	46 ± 4
q	$5.3^{+1.7}_{-1.4}$
a	0.6 ± 0.2
$\xi_{\rm ref}$ [erg cm s^{-1}]	40^{+70}_{-35}
$A_{\rm Fe}$ [solar]	1.5 ± 0.3
$EW_{\rm NL}$ [eV]	13 ± 9
χ^2/d.o.f.	2690/2758

[a]Column density of the intrinsic absorber in units of 10^{21} cm^{-2}.

The ionization state of the reflector is such that the main emission line in the Fe K regime is at 6.4 keV, as suggested already by previous results (we measure $\xi = 40^{+70}_{-35}$ erg cm s^{-1}, while the 6.7 keV Fe line starts to dominate for $\xi \geq 200$ erg cm s^{-1}). The relativistic blurring parameters are consistent with previous results. In particular, we obtain an emissivity index $q = 5.3^{+1.7}_{-1.4}$ and a black hole spin 0.6 ± 0.2, while the inclination is $46° \pm 5°$. In Fig. 4, we show the goodness-of-fit variation as a function of black hole spin. We measure an intermediate spin of $a \simeq 0.6$, but a Schwarzschild solution ($a = 0$) can only be rejected at just the 3σ level. A maximally spinning Kerr black hole is rejected with higher confidence. We must however point out that the $a = 0$ Schwarzschild solution

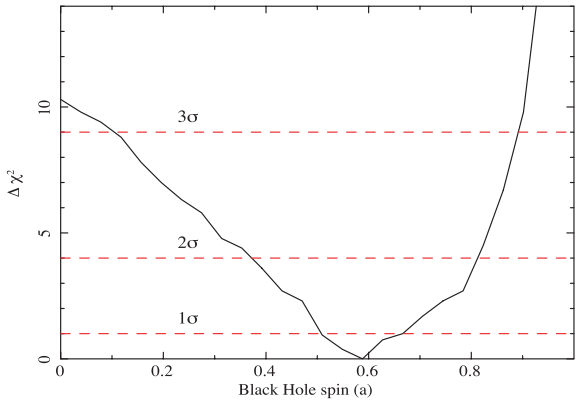

Figure 4. Goodness-of-fit variation as a function of black hole spin. The horizontal lines mark $\Delta\chi^2$=1, 4 and 9, corresponding approximately to 1, 2 and 3σ confidence levels. A value of $a = 0$ is rejected but only just at the 3σ level, while a maximally spinning black hole with $a = 0.998$ can be rejected at the 5σ level (not shown in the figure for clarity, but corresponding to $\Delta\chi^2 = 25.7$).

requires a very steep emissivity $q \geq 5.5$ which would associate all Fe emission with a narrow annulus around the ISCO ($6r_g$), with little contribution from larger radii, which seems highly unlikely.

Despite the result being statistically slightly worse than the previous one, we tend to consider our latest model superior from a physical point of view. In fact, our latest model is particularly appealing because it can describe the whole broad-band X-ray spectrum with a minimal set of well-justified spectral components, namely Galactic and intrinsic absorption, a power-law continuum, and its reflection off the disc (producing the broad relativistic Fe line) and off distant matter (as indicated by the narrow Fe line).

4.4 X-ray variability

So far, we have considered the time-averaged X-ray spectral properties of SWIFT J2127.4+5654. However, NLS1 galaxies are known for their often extreme X-ray variability which is primarily attributed to a relatively small black hole mass. The black hole mass of SWIFT J2127.4+5654 has been estimated by Malizia et al. (2008) to be of the order of $1.5 \times 10^7\,M_\odot$ (see Masetti et al. 2006 for the method). Although this is not a particularly low black hole mass, short time-scale variability should be present if, as indicated by our spectral analysis, X-rays originate in the innermost regions of the accretion flow. As a reference, the light-crossing time of $10r_g$ for the given black hole mass corresponds to a time-scale of ∼700 s. In Fig. 5, we show the XIS 3 light curve in the 0.5–10 keV band (bins of 256 s) which clearly exhibits variability of more than 50 per cent in a few ks with an rms fractional variability of 0.19 ± 0.08.

We have performed time-resolved spectroscopy by selecting 30 intervals of 2–3 ks duration (i.e. the maximum length of uninterrupted data, see Fig. 5) to search for spectral variability and, in particular, to investigate any broad Fe line variability with respect to the continuum. For simplicity, and to avoid any soft excess complication, we restrict our analysis to the 3–10 keV band and we use only the XIS 3 because the lack of sensitivity in the XIS 1 above 7–8 keV prevents us from defining the hard X-ray continuum with the required accuracy. Given the relatively poor quality of the time-resolved data, we use the simplest possible spectral model comprising a power-law continuum and two Gaussian emission lines (one narrow and one broad) modified by an absorbing column of neutral gas fixed at the time-averaged value. All parameters are fixed to the best-fitting values from the time-averaged spectrum, except the photon index, its normalization and the broad-line intensity (see Table 1). Despite this restrictive set of simplifying assumptions, the data are not of good enough quality to claim any significant variation of the broad-line intensity. The continuum photon index is also consistent with being the same throughout the observation. Considering longer time intervals to improve the statistics would wash out most of the short time-scale flux variability, and we then refrain from performing such analysis on the whole observation.

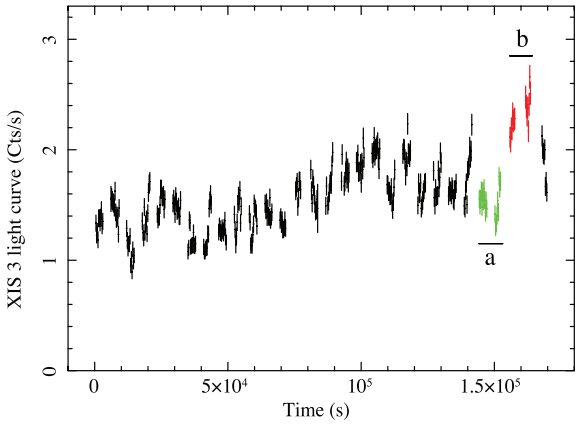

Figure 5. The 0.5–10 keV XIS 3 background subtracted light curve of SWIFT J2127.4+5654. Time bins are of 256 s and only fully exposed bins are used. Intervals (a) and (b) are labelled for reference (see text for details).

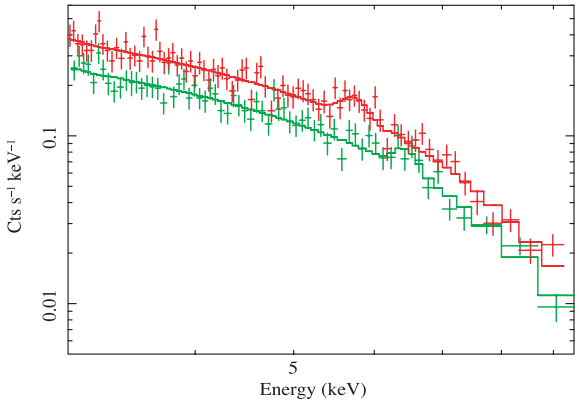

Figure 6. The XIS 3 spectra for intervals (a) (bottom) and (b) (top) as defined in Fig. 5. The bulk of the broad Fe line seems to shift from ∼6.6 keV (a) to ∼5.8 keV (b) in about 10 ks.

The negative result could, however, be due, besides to the low quality of the time-resolved data, to forcing the line parameters to be the same, looking only for a line normalization change. To test for changes in the line profile on short time-scales and with a better signal-to-noise ratio, we have constructed spectra from intervals (a) and (b) shown in Fig. 5 (about 5–6 ks of net exposure each) and applied the same model as before, but now letting all the broad Fe line parameters free to vary. The resulting spectra and best-fitting models are shown in Fig. 6 and indicate the presence of a spectral feature around 5.8 keV in the brighter spectrum only. The Gaussian lines in intervals (a) and (b) are resolved ($\sigma \simeq 150$ eV) and they have energies of $E^{\rm a} = 6.57 \pm 0.10$ keV and $E^{\rm b} = 5.83 \pm 0.12$ keV respectively, and intensities of $I^{\rm a} = 0.35 \pm 0.15 \times 10^{-4}$ ph cm^{-2} s^{-1} and $I^{\rm b} = 0.61 \pm 0.20 \times 10^{-4}$ ph cm^{-2} s^{-1}.

The line parameters are then suggestive of some variability, at least in the centroid energy which is significantly redder in the brighter interval (b). This is visually shown in Fig. 7 where we use the method outlined in Miniutti & Fabian (2006) and show the statistical improvement obtained by running a Gaussian filter through the data for intervals (a) and (b) when both spectra are modelled with the power law plus narrow 6.4 keV Gaussian emission line only. While an additional resolved line is confidently detected in interval (b) at ∼5.8 keV, the detection of the line at ∼6.6 keV during interval (a) is less significant (about 2.5σ). No line at ∼6.6 keV is detected in interval (b), as no line at ∼5.8 keV is seen during interval (a). However, if all broad-line parameters are forced to be the same in the two intervals, the statistical quality of the fit becomes $\chi^2 = 145$ for 145 d.o.f. with respect to $\chi^2 = 135$ for 142 d.o.f. when the broad-line parameters are allowed to be different. The line profile variability is then significant at the ∼98 per cent confidence level only (we also point out that this significance level is likely overestimated since we do not take into account the number of trials for simplicity). We conclude that the data quality is not high enough to study the reflection and Fe line variability in detail, although some tentative evidence for line profile variability is found on time-scales ≤10 ks.

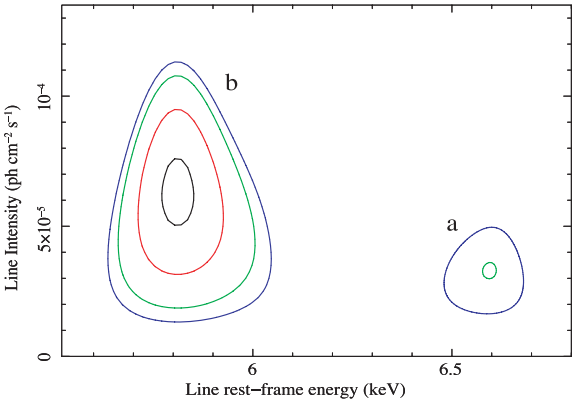

Figure 7. Contours in the intensity–energy plane when a Gaussian filter is applied to the spectra of intervals (a) and (b). The Gaussian has fixed width of 0.1 keV, comparable with the XIS energy resolution, and is varied in the 4–8 keV energy and in the $0 - 4 \times 10^{-4}$ ph cm^{-2} s^{-1} intensity ranges. The contours represent, from outer- to innermost, $\Delta\chi^2 = -4.61$, -6.17, -9.21 and -11.83 with respect to a model when only a power-law continuum and a narrow 6.4 keV Fe line are considered (see Miniutti & Fabian 2006 for details).

Attempting to explain the tentative variability we report is risky (because of its low significance) and we do not want to overinterpret our data. However, assuming that the variability is real, the line appears to be more redshifted in the bright interval. This is opposite to the behaviour predicted, e.g. by the light bending model (see Miniutti & Fabian 2004) which, under the assumption that flux variability is only due to general relativistic effects, associates bright phases with narrower and less redshifted lines. However, other interpretations may be viable and the 5.8 keV line may be associated with the blue peak of an additional line component rather than with the red wing of the broad line (which may be too weak to be confidently detected in the time-resolved intervals). For instance, the bright interval (b) could correspond to a particularly strong X-ray flare above the disc, disconnected from the overall variability trend, and illuminating only a limited off centre region of the disc. The irradiated region then responds with Fe fluorescent line emission with peak energy (and width) dictated by the location and size of the illuminated spot (Dovčiak et al. 2004b), as suggested, e.g., by Iwasawa et al. (1999) in the case of MCG–6-30-15 (see also Iwasawa, Miniutti & Fabian 2004 for an interesting case of flux and energy modulation of such a feature in NGC 3516). The 5.8 keV feature we observe during the bright interval (b) may then be due to a transient flare above the receding part of the inner disc, which potentially explains the relatively large observed redshift of the line.

5 DISCUSSION

We detect with very high significance a broad Fe line in the X-ray spectrum of the NLS1 galaxy SWIFT J2127.4+5654. The line is consistent with being relativistic and most likely originates in reflection from the innermost regions of the accretion disc, close to the central black hole. The good quality of our *Suzaku* observation is sufficient to provide a measure of the black hole spin in SWIFT J2127.4+5654, a relatively rare opportunity in AGN studies.

The black hole in SWIFT J2127.4+5654 appears to be a rotating Kerr black hole with an intermediate spin of 0.6 ± 0.2. A non-rotating Schwarzschild black hole ($a = 0$) is statistically rejected but just at the 3σ level, while a maximally rotating Kerr one ($a = 0.998$) can be excluded at the 5σ level (Fig. 4). Since a black hole having accreted a significant fraction of its mass should spin at very high rate (Volonteri et al. 2005) accretion in SWIFT J2127.4+5654 might proceed through short episodes with random hole–disc angular momentum alignment. Accretion could then either add or remove angular momentum depending on the relative orientation in each accretion episode. The current accretion episode should be short enough to prevent the hole from having accreted a significant fraction of its mass thus reaching maximal or nearly maximal spin. If we assume a typical efficiency of 0.1, and given that SWIFT J2127.4+5654 has a bolometric luminosity of $\sim 3.5 \times 10^{44}$ erg s^{-1} (see Table 1) for a black hole mass of $\sim 1.5 \times 10^7$ M$_\odot$, the black hole in SWIFT J2127.4+5654 can double its mass in about 0.2–0.3 Gyr. This sets a conservative upper limit for the duration of the accretion episode that is powering the AGN in SWIFT J2127.4+5654.

We must point out that our spin measurement is based on the assumption that the reflecting disc is truncated at the ISCO. This assumption is reasonable, but can introduce a systematic error on the inferred spin value if the disc is truncated near but not exactly at the ISCO, i.e. if material in the plunging region beyond the ISCO can still act as a reflector with low enough ionization to produce an observable contribution to the reflection spectrum. Recent numerical simulations suggest that the uncertainty in the reflector inner edge could at most reduce the spin we have inferred by ~ 0.2 (Reynolds & Fabian 2008). A lower black hole spin would only add strength to the previous argument, favouring short-lived accretion episodes in SWIFT J2127.4+5654 as opposed to prolonged accretion. Given that counter-rotating discs spin down black holes more efficiently than co-rotating discs spin them up because gas particles leaving the ISCO to plunge towards the black hole have larger angular momenta in the counter-rotating case (see Bardeen 1970; Bardeen, Press & Teukolsky 1972), the black hole spin distribution in this scenario should be skewed towards low values. King et al. (2008), who investigated in detail the effect of chaotic accretion episodes on the black hole spin, conclude indeed that the spin distribution for black holes of $\sim 10^7$ M$_\odot$ should peak around $a = 0.2$–0.3 with a spread $\Delta a \simeq 0.2$, broadly consistent with our measurement, especially if the correction due to the uncertainty in the reflector inner edge is considered.

The second relevant result we have obtained concerns the shape of the reflection emissivity profile. We measure a rather steep index $q \simeq 5$ with a 90 per cent lower limit $q \geq 3.9$. A powerful and centrally concentrated irradiating X-ray source is required to achieve such steep profiles, possibly related to the magnetic extraction of the black hole rotational energy via magnetic fields (see e.g. Wilms et al. 2001 for a discussion). Relativistic light bending may also contribute to focus the irradiating X-rays towards the innermost disc regions, thus inducing an effective steeper emissivity (Miniutti & Fabian 2004). Here we stress that the emissivity index q and the black hole spin are somewhat degenerate in spectral fitting: as shown in Fig. 2, a steep emissivity profile tends to force low values of spin (or large values of the inner radius). Therefore, we detect a spin $a > 0$ despite (and not because of) a steep emissivity. Moreover, from a physical point of view, if the steep profile is indeed associated with the extraction of the black hole rotational energy (plus light bending), steep emissivity profiles should only be obtained for $a > 0$.

Rotational energy extraction tends to reduce the black hole spin, thus representing a possible alternative to chaotic accretion as an explanation for the intermediate spin we measure. If we assume prolonged accretion (which tends to force a maximally spinning

hole) and rotational energy extraction (which tends to spin the hole down) via the Blandford & Znajek (BZ) mechanism (Blandford & Znajek 1977), the black hole spin evolution is different than with accretion alone, and an equilibrium spin value is reached. It is interesting to note that Moderski & Sikora (1996), who analysed in some detail the interplay between accretion and BZ mechanism in building up the black hole spin, predict an equilibrium spin of $a_{\rm eq} \sim 0.6$ if the current mass accretion rate (in terms of Eddington, see Table 1) of SWIFT J2127.4+5654 and a standard α-viscosity parameter of 0.1 are assumed. This estimate is actually remarkably consistent with our spin measurement. We then consider it plausible that accretion in SWIFT J2127.4+5654 is prolonged, but that the spin is limited by rotational energy extraction which may power the X-ray source. Such occurrence may explain simultaneously the spin value and the steep emissivity profile we infer from our spectral analysis. Besides a possible recent merger, the intermediate spin of SWIFT J2127.4+5654 is then consistent with two competing scenarios, namely (i) chaotic accretion episodes or (ii) prolonged accretion plus rotational energy extraction via magnetic mechanisms.

Tentative line profile variability is seen on time-scales $\leq$10 ks. Confirming such short time-scale variability in this and other similar sources with broad lines would allow us to confidently rule out any competing spectral model (such as complex absorption) and to probe the relativistic regime around supermassive black holes. Continuous data sets would be very helpful in assessing the variability on short time-scales (e.g. observations with *XMM–Newton*). On the other hand, a very significant improvement in effective area at $\sim$6 keV with respect to current observatories is necessary to probe the shortest time-scales. Considering that the XIS 3 effective area is $\sim$220 cm^2 at 6 keV, $\sim$1 m^2 is required to perform time-resolved spectroscopy of bright X-ray sources on time-scales shorter than the orbital one in the inner disc. Future missions such as the International X-ray Observatory (IXO) will be ideal to probe without ambiguity and with great accuracy the accretion flow properties in the relativistic region.

ACKNOWLEDGMENTS

GM thanks the Spanish Ministerio de Ciencia e Innovación and CSIC for support through a Ramón y Cajal contract. ACF thanks the Royal Society for support. FP acknowledges support from the Italian Space Agency (ASI) grant ASI/I/008/07.

REFERENCES

Arnaud K. A., 1996, in Jacoby G. H., Barnes J., eds, ASP Conf. Ser. Vol. 101, Astronomical Data Analysis Software and Systems V. Astron. Soc. Pac., San Francisco, p. 17
Balucinska-Church M., McCammon D., 1992, ApJ, 400, 699
Bardeen J. M., 1970, ApJ, 161, 103
Bardeen J. M., Press W. H., Teukolsky S. A., 1972, ApJ, 178, 347
Bautista M. A., Kallman T. R., 2001, ApJS, 134, 139
Berti E., Volonteri M., 2008, ApJ, 684, 822
Bianchi S., Guainazzi M., Matt G., Fonseca Bonilla N., Ponti G., 2009, A&A, 495, 421
Blandford R. D., Znajek R. L., 1977, MNRAS, 179, 433
Brenneman L. W., Reynolds C. S., 2006, ApJ, 652, 1028
Condon J. J. et al., 1998, AJ, 115, 1693
Dorman B., Arnaud K. A., 2001, ASP Conf. Proc. Vol. 238, Astron. Soc. Pac., San Francisco, p. 415
Dovčiak M., Karas V., Yaqoob T., 2004a, ApJS, 153, 205
Dovčiak M., Bianchi S., Guainazzi M., Karas V., Matt G., 2004b, MNRAS, 350, 745
Fabian A. C., Miniutti G., 2009, in Wiltshire D. L., Visser M., Scott S. M., eds, The Kerr Spacetime. Cambridge Univ. Press, Cambridge
Fabian A. C., Rees M. J., Stella L., White N. E., 1989, MNRAS, 238, 729
Fabian A. C., Iwasawa K., Reynolds C. S., Young A. J., 2000, PASP, 112, 1145
Fabian A. C. et al., 2002, MNRAS, 335, L1
George I. M., Fabian A. C., 1991, MNRAS, 249, 352
Halpern J. P., 2006, Astron. Telegram, 847, 1
Iwasawa K., Fabian A. C., Young A. J., Inoue H., Matsumoto C., 1999, MNRAS, 306, L19
Iwasawa K., Miniutti G., Fabian A. C., 2004, MNRAS, 355, 1073
Kalberla P. M. W., Burton W. B., Hartmann D., Arnal E. M., Bajaja E., Morras R., Pöppel W. G. L., 2005, A&A, 440, 77
King A. R., Pringle J. E., Hofmann J. A., 2008, MNRAS, 385, 1621
Komossa S., Voges W., Xu D., Mathur S., Adorf H.-M., Lemson G., Duschl W. J., Grupe D., 2006, AJ, 132, 531
Koyama K. et al., 2007, PASJ, 59, 23
Laor A., 1991, ApJ, 376, 90L
Makishima K., Maejima Y., Mitsuda K., Bradt H. V., Remillard R. A., Tuohy I. R., Hoshi R., Nakagawa M., 1986, ApJ, 308, 635
Malizia A. et al., 2008, MNRAS, 389, 1360
Marconi A., Risaliti G., Gilli R., Hunt L. K., Maiolino R., Salvati M., 2004, MNRAS, 351, 169
Masetti N. et al., 2006, A&A, 459, 21
Miller J. M., 2007, ARA&A, 45, 441
Miller J. M., Reynolds C. S., Fabian A. C., Miniutti G., Gallo L. C., 2009, ApJ, 697, 900
Miniutti G., Fabian A. C., 2004, MNRAS, 349, 1435
Miniutti G., Fabian A. C., 2006, MNRAS, 366, 115
Miniutti G. et al., 2007, PASJ, 59, 315
Miniutti G., Ponti G., Greene J. E., Ho L. C., Fabian A. C., Iwasawa K., 2009, MNRAS, 394, 443
Moderski R., Sikora M., 1996, MNRAS, 283, 854
Reynolds C. S., Fabian A. C., 2008, ApJ, 675, 1048
Reynolds C. S., Nowak M. A., 2003, Phys. Rep., 377, 389
Ross R. R., Fabian A. C., 2005, MNRAS, 358, 211
Sikora M., Stawarz L., Lasota J. P., 2007, ApJ, 658, 815
Takahashi T. et al., 2007, PASJ, 59, 35
Tueller J. et al., 2005, Astron. Telegram, 669, 1
Turner T. J., Miller L., 2009, A&AR, 17, 47
Volonteri M., Madau P., Quataert R., Rees M. J., 2005, ApJ, 620, 69
Wilms J., Allen A., McCray R., 2000, ApJ, 542, 914
Wilms J., Reynolds C. S., Begelman M. C., Reeves J., Molendi S., Staubert R., Kendziorra E., 2001, MNRAS, 328, L27

This paper has been typeset from a TEX/LATEX file prepared by the author.